RESEARCH   **Open Access**

Shear Capacity Contribution of Steel Fiber Reinforced High-Strength Concrete Compared with and without Stirrup

Tian-Feng Yuan[1], Doo-Yeol Yoo[2], Jun-Mo Yang[3] and Young-Soo Yoon[1*]

Abstract

This study presents the shear capacity of eco-friendly high-strength concrete (HSC) beams reinforced by 0.75% (by volume) of hooked steel fibers or shear stirrups with various spacings. Five large-scale HSC beams with steel fibers or stirrups were tested and investigated with respect to shear capacity, failure mode, and crack patterns. The test results indicate that all five tested beams finally failed by a shear-critical failure mode and that the use of 0.75 vol% of steel fibers significantly improved the shear strength although it decreased the diagonal crack angle of HSC beam in the case of without stirrups. There are some different properties compared with ACI 318-19 recommendation, but the use of 0.75 vol% steel fibers exhibited approximately 13.2% higher shear strength when compared with that of minimum shear reinforcement for the HSC beam. Furthermore, the shear capacity of steel fibers calculated by experimental data, and it was compared with several prediction equations. The prediction models containing fiber factor were more closely agreeable with test results with a minimum of 10.9% difference.

Keywords: shear capacity, hooked steel fiber, stirrups, high-strength concrete

1 Introduction

In the context of the fourth industrial revolution, more and more emphasizes the using environmental friendly construction methods and sustainable materials. The main issue of construction is devote to achieve energy saving and reduce materials cost, energy consumption and carbon dioxide emission. Therefore, many of researchers have focus on the development of alternative binders to Portland cement. The alternative binders are generally using industrial waste products such as ground granulate blast furnace slag (GGBFS) and fly ash with latent hydraulic property (Zezulka et al. 2016; Oesterreich and Teuteberg 2016; Yang et al. 2017). In particular, various replace Portland cement ratios of GGBFS were widely investigated, and it have better mechanical

properties as compared to conventional Portland cement base concrete (Yang et al. 2017; Yuan et al. 2018). Furthermore, for improve the toughness and ductility of concrete using GGBFS, various fiber types and volume ratios were adopted according to conventional fiber reinforced concrete (FRC).

In the late 1970s, fiber-reinforced concrete (FRC) was widely researched and used in construction, which was reported that increase in post-cracking behavior, tensile strength, toughness, ductility, and energy absorption (Yang et al. 2017; Fettu 2008; Prisco et al. 2009). In the other words, base on transfer stress across cracks of steel fibers mechanism, prevent crack development and large crack widths, improve shear resistance and stiffness, and decrease deflections of reinforced concrete (RC) beams.

The many authors investigated fiber contribution in the RC beams and compared steel rebar reinforcement with steel fiber reinforcement and without stirrups to resist shear load (Tan et al. 1993; Aoude et al. 2012; Narayan and Darwish 1987; Cucchiara et al. 2004). The authors

observed that the steel fiber reinforcement concrete beams exhibited a similar crack pattern and an almost increase in the ultimate average shear strength, and the increases in the fiber volume fraction increase shear resistance capacity. Additionally, a few studies investigated the feasibility of replacing the minimum shear reinforcement with discontinuous steel fibers as mentioned by using a certain admixture ratio of steel fiber in RC beams to replace the minimum shear reinforcement (Minelli and Plizzari 2013; Parra-Montesinos and Wight 2006). Previous studies (Parra-Montesinos and Wight 2006; ACI Committee 318 2019) investigated and summarized the amount of shear test data wherein the use of minimum fiber volume fraction of 0.75% in RC beams led to a shear capacity that exceeded $0.30\sqrt{f_{ck}}$ (MPa), and thus the use of 0.75 vol% steel fibers can replace minimum shear reinforcement. Subsequently, a few studies investigated and verified the feasibility of replacing the minimum shear reinforcement with steel fibers in normal and high strength concrete (Yoo et al. 2017). The authors investigated the feasibility of eliminating the minimum shear reinforcement in reinforced sustainable high strength concrete beams by using 0.75 vol% of hooked steel fibers under a flexural bending test. All the test specimens (three different sizes of test beams) exhibited flexural failure mode which were reinforced by using 0.75 vol% of steel fibers without stirrups or reinforcing the minimum stirrups without steel fibers. Therefore, several studies proposed prediction equations to evaluate the contribution of steel fibers on the shear strength base on experimental test data (Aoude et al. 2012; Noghabai 2000; Foster 2010; Bentz et al. 2006; Abu-Lebdeh et al. 2011; Lantsoght 2019).

Although several studies investigate the fiber contribution in the flexure and shear behaviors, there is a less of studies that investigate increments in shear capacity by comparing shear reinforcement by using 0.75 vol% of steel fibers without stirrups and only by using stirrups. Especially, shear properties of eco-friendly high strength concrete containing 60% GGBFS and reinforced by steel fiber, based on the structural point of view, still needs further investigation. It is necessary to perform a quantitative evaluation and investigate the shear behavior of hooked steel fiber reinforced HSC beam under a larger-scale size test. Therefore, in this study, in order to investigate the shear capacity of hooked steel fibers in HSC beam, the HSC beam that is only reinforced by 0.75 vol% of hooked steel fibers and four large beams with different spacings of shear reinforcement (stirrups) were fabricated. Additionally, the shear strengths of fiber contribution behavior were compared between the experimental and prediction equations.

2 Experimental Program

In this study, five large-scale test beams were prepared by using eco-friendly high strength concrete (HSC) with and without steel fibers or shear reinforcement. The hooked steel fiber with a fiber volume fraction of 0.75%, and shear reinforcement ratios of 0.0 (0.0*d*), 0.32 (0.25*d*), 0.21 (0.375*d*) and 0.16 (0.5*d*) were adopted. All the HSC beams were tested under four-point flexural loads. And the compressive strength and four-point bending tests of HSC with and without steel fibers were investigated. Furthermore, for evaluating shear strength capacity base on the prediction equations, the fiber pullout test and three-point notch bending test were performed. The details of HSC with and without steel fibers mixture proportions, materials, test beams, mechanical test and test setup performed in this study are as follows.

2.1 Mixture Proportions and Materials

The mixture properties of HSC beams are listed in Table 1. TypeI Portland cement (a specific surface area of 3413 cm^2/g and a density of 3.15 g/cm^3, produced by the Republic Korea), Type III GGBFS (a specific surface area of 4250 and a density of 2.90 g/cm^3, produced by the Republic Korea) were used. The chemical and physical properties of these materials are listed in Tables 2, 3. The water to binder ratio (*w/b*) of 27.5% and GBFS replacement ratios of 60 wt% of cement were adopted. And the fine aggregate was obtained by using crushed aggregate, and the gravel with a maximum aggregate size of 20 mm was used with a coarse aggregate. Additionally, a polycarboxylate superplasticizer (SP) with a density of 1.06 g/cm^3 was used to improve the suitable fluidity. Hooked steel fiber with a fiber volume fraction of 0.75% was used, and the fiber exhibited the following characteristics: a length of 35 mm, equivalent diameter of 0.55 mm, and nominal tensile strength of 1400 MPa. The physical and

Table 1 Proportion of materials in the HSC mixture.

	w/b (%)	GBFS/B (%)	s/a(%)	Cement	Water	BFS	Fine aggregate	Coarse aggregate	SF (vol%)	SP (%)
HSC-N	27.5	60	42.4	1.00	0.69	1.50	2.83	3.86	–	0.5
HSC-SF									0.75	1.0

w/b = water-to-binder ratio, GBFS/B = ratio of granulated blast furnace slag and total binder, s/a = ratio of amount of fine aggregate to total amount of aggregate, GBFS = granulated blast furnace slag, SF = hooked steel fiber by volume of HSC, and SP = superplasticizer.

Yuan *et al. Int J Concr Struct Mater*   (2020) 14:21

Page 3 of 15

Table 2 Chemical compositions and physical properties of cement.

Surface area (cm²/g)	Density (g/cm³)	Ig.loss (%)	Chemical composition (%)					
			SiO$_2$	Al$_2$O$_3$	Fe$_2$O$_3$	CaO	MgO	SO$_3$
3413	3.15	1.40	21.25	5.28	3.02	61.00	3.71	1.24

Table 3 Chemical compositions and physical properties of GBFS.

Surface area (cm²/g)	Density (g/cm³)	Ig.loss (%)	Chemical composition (%)		
			SiO$_2$	MgO	Cl$^-$
4250	2.90	0.32	21.01	6.40	0.005

geometrical properties of the fiber are separately listed in Table 4.
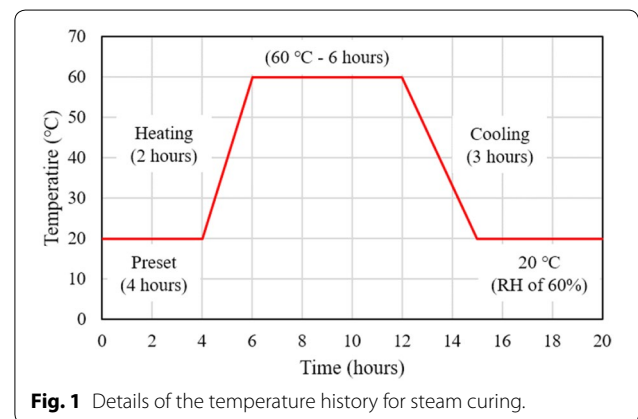
Furthermore, the steam curing condition was adopted to accelerate the strength development of HSC. For the first 4 h (hours), all the test specimens were cured at approximately 20 ± 1 °C and a relative humidity (RH) of $60 \pm 5\%$. Subsequently, the curing temperature increased from 20 ± 1 to 60 ± 5 °C according to 2 h with steam, and a high constant temperature of 60 ± 1 °C was maintained for 6 h. The high temperature was then reduced from 60 to 20 °C according to 3 h, and all the specimens were cured at constant temperature 20 ± 1 °C and an RH of $60 \pm 5\%$ for a period of 28 days after the HSC casting. The details of temperature history for steam curing process are shown in Fig. 1.

2.2 Details of the Mechanical Test and Specimen Preparation

For compressive strength, three cylindrical specimens with a diameter of 100 mm and a height of 200 mm were cast based on ASTM C39 (2014). In order to measure the strain capacity and elastic modulus in the compressive strength test, a compressor meter equipped with three linear variable differential transformers (LVDTs) were used. Additionally, three prism specimens with a height of 100 mm, a width of 100 mm, a span of 300 mm, and length of 400 mm were cast for flexure strength based on four-points bending tests of ASTM C1609 (2012). Each prism specimen was turned

90° from the casting surface and then failed completely at mid-span. In order to eliminate the mid-span deflection capacity of prism specimens, a specialized steel frame with two LVDTs were attached to the prismatic specimens on the each side. The loading condition of compressive and flexure strength tests were switched to displacement control at rates of 0.1 mm/min and 0.2 mm/min, respectively.

Furthermore, to calculate shear strength of HSC reinforcement with steel fibers using prediction equation, a simple three-point flexural bending test was proposed based on RILEM TC 162-TDF (2000a). For this, three notched prism specimens with height and width of 150 mm, and a length of 550 mm were fabricated (Fig. 2a). All the mechanical tests were performed by using a universal testing machine (UTM) with a capacity of 2500 kN. To investigate the bond behavior of hooked steel fiber in HSC matrix, a single fiber pullout test was performed (Won et al. 2013). The six dog-bone-shaped specimens were fabricated, and the specimen was divided into two parts, and the fiber was implanted in the center. The test was performed by using a 50 kN UTM with displacement control at a rate of 0.4 mm/min (Fig. 2b).

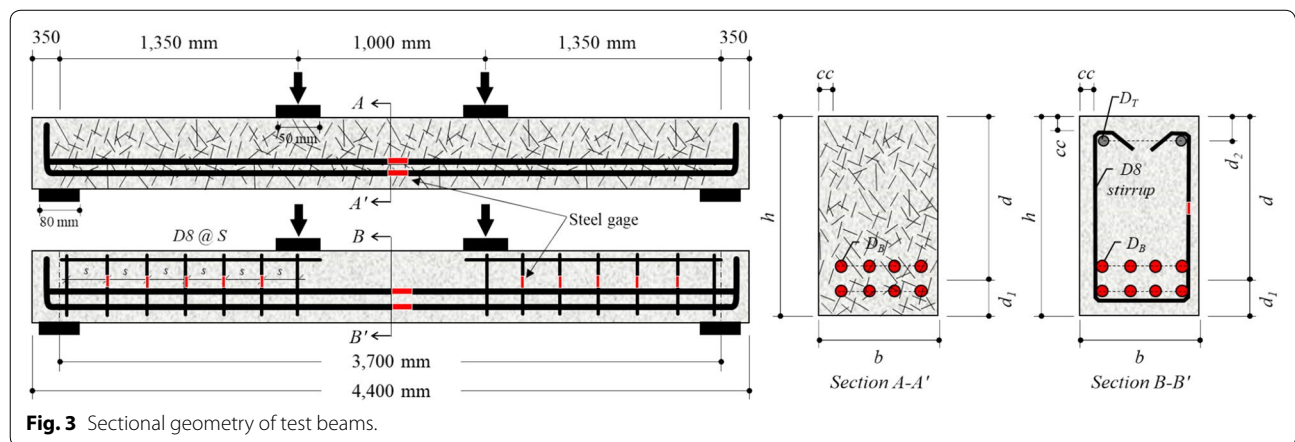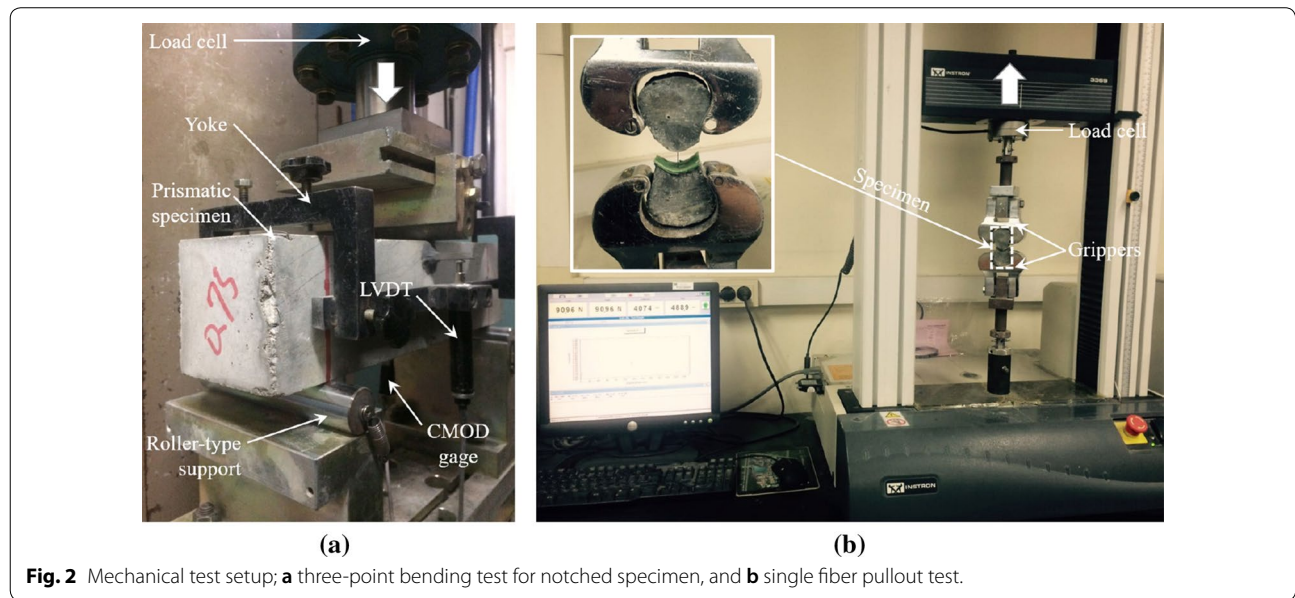**Fig. 1** Details of the temperature history for steam curing.

Table 4 Properties of hooked-end steel fibers.

	Diameter, d_f (mm)	Length, l_f (mm)	Aspect ratio (l_f/d_f)	Density (g/cm³)	Tensile strength (MPa)	Elastic modulus (GPa)
Hooked-end steel fiber	0.55	35	65	7.9	1400	200

2.3 Details of Beam Specimens and Test Setup

The experimental shear test prepared a total of five large-scales HSC beam specimens with rectangular cross-sections. Five beam specimens with different amounts of shear reinforcement or steel fibers and details are shown in Fig. 3 and summarized in Table 5. The specimen with

0.75 vol% of hooked-end steel fibers and without shear reinforcement (HSC-SF) was prepared for the investigation, which the purpose involves resisting shear failure equivalent to replace the minimum shear reinforcement through the use of steel fibers as recommended by ACI 318-19 (2019). The other specimens involved the use of

(a)   **(b)**

Fig. 2 Mechanical test setup; **a** three-point bending test for notched specimen, and **b** single fiber pullout test.

Fig. 3 Sectional geometry of test beams.

Table 5 Dimensions of reinforced HSC beams.

	D_T	D_B	h (mm)	b (mm)	d (mm)	d_1 (mm)	d_2 (mm)	$Av/(bs)$	s (mm)	cc (mm)
NS-N	D8	D25	500	300	442	58	27	–	–	–
105S-N	D8	D25	500	300	442	58	27	0.32	105	20
158S-N	D8	D25	500	300	442	58	27	0.21	158	20
210S-N	D8	D25	500	300	442	58	27	0.16	210	20
NS-SF	D8	D25	500	300	442	58		–	–	–

Yuan *et al. Int J Concr Struct Mater*   (2020) 14:21

Page 5 of 15

plan concrete (HSC-N) and designed different spacing of shear reinforcement to evaluate the effect of stirrup spacing on the shear resistance of HSC beams by varying shear reinforcement ratios as 0.0, 0.16, 0.21 and 0.32. The shear reinforcement ratios of 0.16 is the minimum shear reinforcement. Additionally, in order to prevent bending failure and pullout at the end of the beam, 8 D25 of SD400 steel rebars with a yield strength of approximately 491 MPa were used, and an end of longitudinal steel reinforcing rebars with a hook was applied to all test beams. With respect to the five large-scale beams, were calculated longitudinal reinforcement ratios unify at 3.15%, which calculated a value based on $A_s/b_w d$, where A_s, b_w, and d denote the area of rebars, width, and effective depth of the beam, respectively. Additionally, the dimensions of five large-scale beams were as follows: a beam width of 300 mm, a height of 500 mm, and a length of 4400 mm. The physical and geometrical properties of the steel rebars are separately listed in Table 6. The system used to designate the specimens was as follows: the letters N and SF denote without and with hooked-end steel fibers, respectively, the letters S and NS denote with and without shear reinforcement, respectively.

The beams were tested under a four-point loading condition, and the load was applied to the test beams as two equal concentrated loads distance of 1000 mm. All the specimens were supported by pins with an edge distance of 350 mm at both ends. Therefore, the shear span-depth ratio (a/d) is maintained as 3.05 and leads to significant shear failure under the four-point loading test, where a denotes shear span length. It is based on a decrease in the shear resistance capacity with increases in a/d and almost no change when a/d exceeds 3.0 when all other factors are equal. The load cell, LVDTs, and steel strain gages were used to measure the applied load, displacement at mid-span, and strain of reinforcement, respectively. The LVDTs were set to mid-span and under the loading points to measure pure mid-span deflections. Several steel strain gages were embedded in the center of longitudinal and shear reinforcing rebars to measure the state of strain at different load magnitudes. Additionally, the loading condition of large-scale beam test was switched to displacement control at a rate of 0.3 mm/min, which was using a UTM of 2000 kN maximum capacity to apply the monotonic loading. All the instrumentation appliance was connected to data log to record the real-time data during the testing process until shear failure occurred with a significant reduction in the load-carrying capacity. The number and patterns of cracks were obtained at planed load magnitudes during the testing, and the crack width was recorded by using a crack width comparator. Figure 4 shows the details of the beam specimens, set up, and basic types of instrumentation used in the present study.

3 Test Results and Discussion
3.1 Mechanical Properties
Table 7 summarizes the average strength, elastic modulus, strain capacity (strain at the peak strength) and deflection capacity based on compressive and flexural strength test. A minimum of three HSC cylindrical and prism specimens were prepared and tested at 28 days.

The HSC-N (without fibers) compressive strength, elastic modulus, and strain capacity were observed as 67.0 MPa, 32.0 GPa, and 0.00310 mm, respectively. The HSC-SF (with 0.75 vol% steel fibers) exhibited excellent mechanical properties that exceed those of HSC-N approximately 6.9%, 2.8%, and 4.9%, respectively (Table 7). The addition of steel fibers improves energy dissipation capacity, inhibits crack propagation and development in the concrete matrix, and ensure that the steel fiber reinforced specimens are not crushed completely after crack (Yang et al. 2017; Naaman and Reinhardt 2006; Sahoo et al. 2015; Ezeldin and Balaguru 1992).
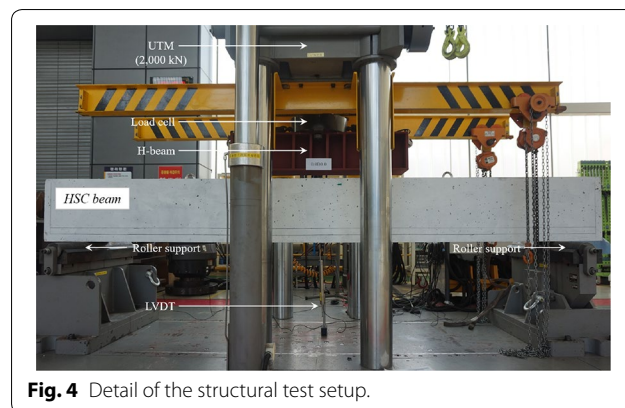

Fig. 4 Detail of the structural test setup.

Table 6 Properties of steel reinforcing bars.

	Name	d_s (mm)	A_s (mm²)	f_y (MPa)	E_s (GPa)	ε_y (mm/mm)
Longitudinal reinforcement	D25	25.4	506.7	491	200	0.002455
Transverse reinforcement	D8	8.0	50.3	466	200	0.002330

d_s = diameter of rebar, A_s = area of rebar, f_y = yield strength, E_s = elastic modulus, ε_y = yield strain.

Table 7 Mechanical properties of concrete.

	Compressive strength test				Flexural tensile strength				
	f_{ck} (MPa)		E_c (GPa)	ε_c (mm/mm)	f_{LOP} (MPa)		f_{MOR} (MPa)		δ_{MOR} (mm)
	Mean	*S.D*			*Mean*	*S.D*	*Mean*	*S.D*	
HSC-N	67.0	5.1	32.0	0.00310	7.0	0.2	7.0	0.2	0.063
HSC-SF	72.0	2.1	32.9	0.00326	9.2	0.2	10.0	0.2	0.870

f_{ck} = compressive strength, S.D. = standard deviation, E_c = elastic modulus, ε_c = strain at the peak strength, f_{LOP} = first cracking flexural strength, f_{MOR} = post-cracking flexural strength, δ_{MOR} = deflection capacity.

The flexural strength test results exhibited that in a manner similar to compressive strength tests, the HSC-SF exhibited higher first cracking flexural strength, post-cracking flexural strength, and deflection capacity corresponding to 9.2 MPa, 10.0 MPa, and 0.870 mm, respectively, which exceed those of HSC-N by approximately 31.4%, 42.9%, and 130%, respectively. The values of the first cracking flexural strength and post-cracking strength was exhibited same value in the HSC-N specimen, since the load-carrying capacity of HSC-N specimen suddenly decreased to almost zero immediately after matrix cracking. In contrast, the HSC-SF specimens exhibited increasing load-carrying capacity after matrix cracking, and this termed as deflection-hardening behavior. It is attributed to the bridge effect of the steel fiber that significantly increases post-crack resistance at the crack surface.

Furthermore, the curve of flexural load versus deflection of prism specimen under three-point flexure is shown in Fig. 5b. According to the RILEM TC 162-TDF recommendation, the equivalent flexural strength strengths ($F_{eq,2}$, $F_{eq,3}$), and the energy absorption capacities ($D^f_{DZ,2}$, $D^f_{DZ,3}$) were calculated, which were approximately 9.15 MPa, 7.05 MPa, 14.3 kN mm, 55.1 kN mm, respectively. Figure 5c shows the typical load–displacement curve for the pull-out load of the test sample reinforced with one fiber in HSC using hooked steel fiber, and the average bond stress was exhibited 6.16 MPa at 28 days. It was exhibited great bond stress according to reported by researchers (Grünewald 2004), which range of bond stress was 5.0–6.0 MPa when compressive strength over 70 MPa.

Hence, according to the fiber bridging effect in the matrix, the HSC with steel fibers (HSC-SF) exhibited higher strength (compressive strength and flexural strength), strain capacity, elastic modulus, post-peak ductility, and deflection capacity relative to the HSC-N.

3.2 Shear Tests for Reinforced HSC Beams with and Without Steel Fibers and stirrups
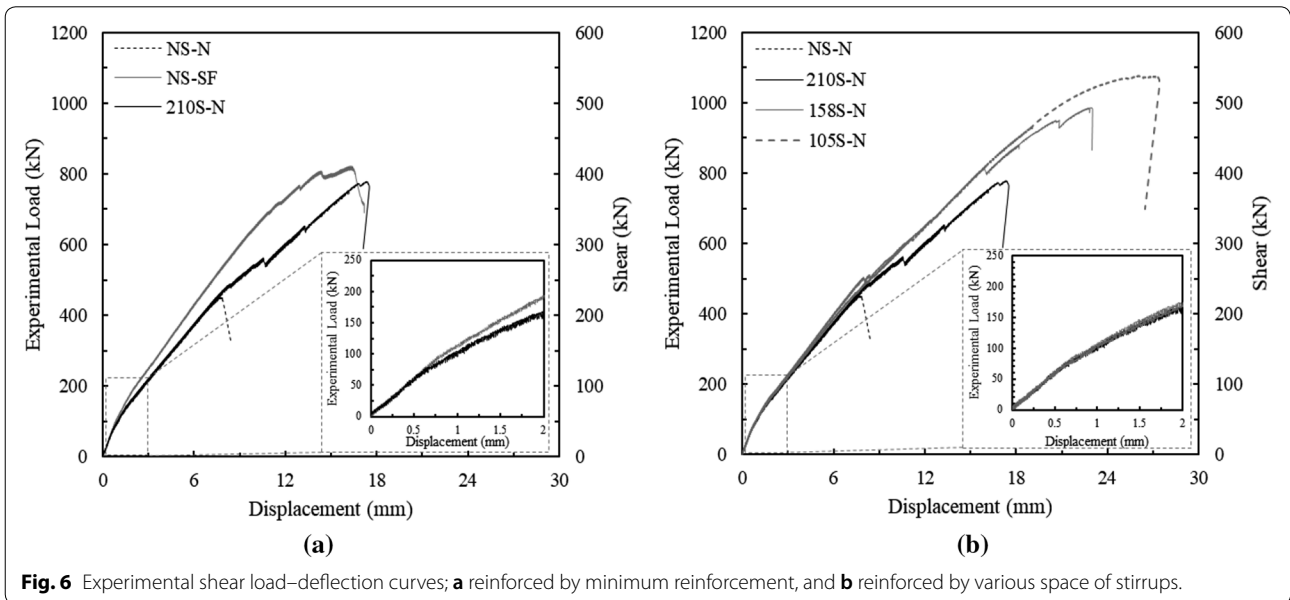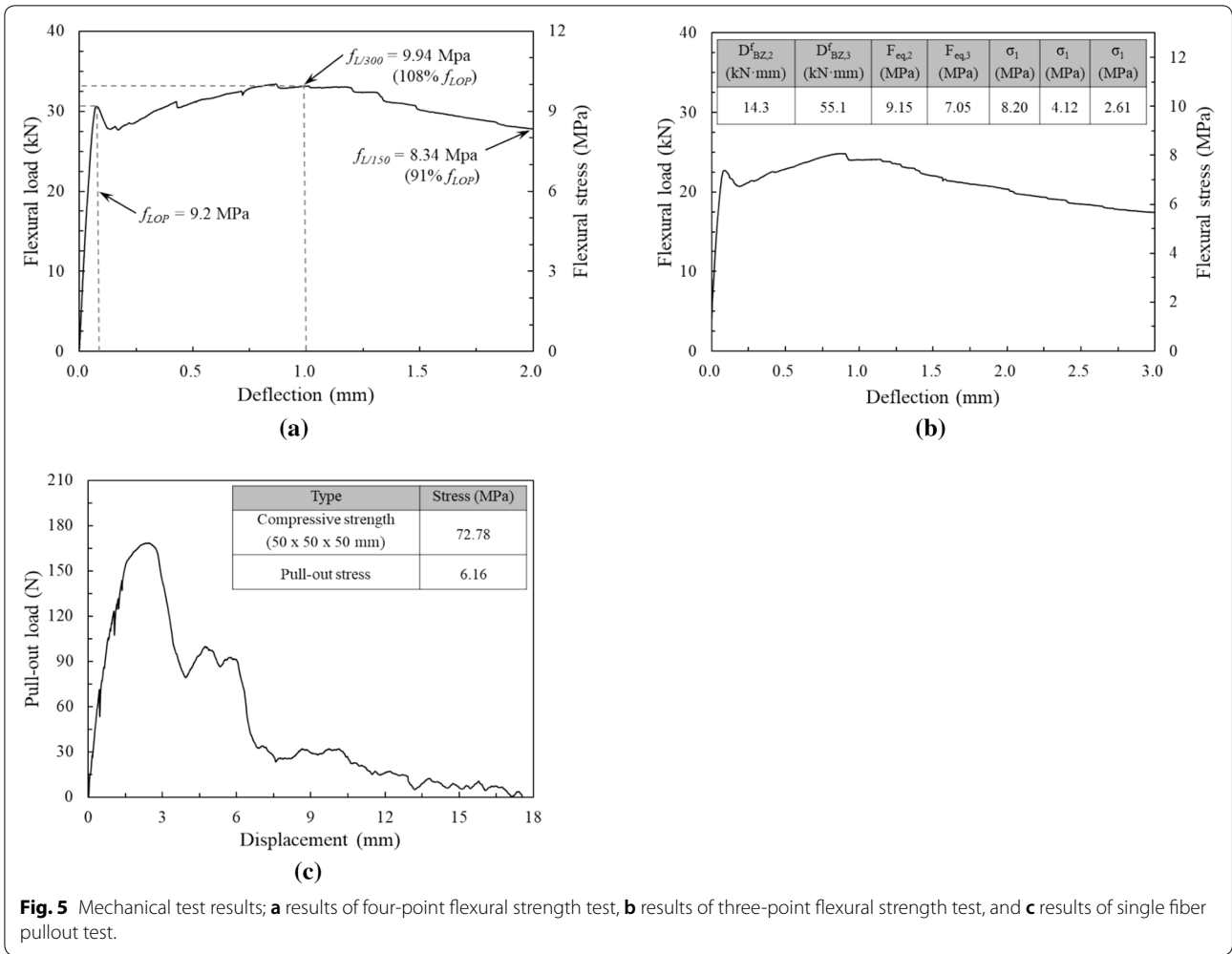
3.2.1 Load–Displacement Response

A comparison of the load relative to mid-span deflection behaviors for the test beam specimens are shown in Fig. 6. Table 8 compares the values for the observed load of initial shear crack V_{cr}; maximum shear capacity $V_{u,exp}$; deflection at peak load δ_u; average maximum strain of longitudinal reinforcement measured by strain gages at the bottom layer of the mid-span ε_L; maximum strain of shear reinforcement by the strain gage at the outside of the center layer ε_T; and measured angle of the inclination of the critical shear crack at beam mid-height θ_{exp}. The load of initial shear crack (V_{cr}) is the value of load at the end of the initial linear zone in the load relative to the deflection curve.

As shown in Fig. 6, for all the tested beam specimens, the initial strains in longitudinal steel rebars were proportional to the load and increased linearly due to the occurrence of cracks, and the nonlinear load-strain curve occurred after the initial shear crack until beam failure. The bottom layer of the longitudinal reinforcement experienced mostly below the yielding value capacity ($\varepsilon_L \leq \varepsilon_{sy}$), and thus the final failure mode of the specimens was a shear failure.

The Fig. 6a compares the load relative to the deflection behavior of beams prepared with HSC (NS-N) and reinforced by minimum shear reinforcement (210S-N) or steel fibers (NS-SF). The specimens NS-N without shear reinforcement and steel fibers exhibited the lowest ultimate shear strength and deflection capacities (deflection at the peak load), such as 226.0 kN and 7.70 mm, respectively. The specimen reinforced by using minimum shear reinforcement (210S-N) or 0.75 vol% steel fibers (NS-SF) increased the ultimate shear strength by approximately 72.3% and 81.9% and deflection capacity of specimen NS-N by 1.3 times. The NS-SF specimen exhibited higher stress at the initial shear crack and an ultimate shear strengths of 56.2 kN and 411.1 kN, respectively, and these are approximately 22.5% and 5.6%, respectively, higher when compared with those of specimen 210S-N. Additionally, specimen NS-SF exhibited higher stiffness and lower deflection when compared with 210S-N. Due to the fibers, increased flexural stress and stiffness after cracking was achieved along with more effective control of cracking.

Fig. 5 Mechanical test results; **a** results of four-point flexural strength test, **b** results of three-point flexural strength test, and **c** results of single fiber pullout test.

Fig. 6 Experimental shear load–deflection curves; **a** reinforced by minimum reinforcement, and **b** reinforced by various space of stirrups.

Table 8 Summary of beam test results.

	V_{cr} (kN)	$V_{u,exp}$ (kN)	δ_u (mm)	ε_L (mm/mm)	ε_T (mm/mm)	θ_{exp} (°)	Failure mode
NS-N	51.4	226.0	7.70	0.001326	–	42	Shear
105S-N	30.4	537.8	29.44	0.008573	0.002437	52	Shear
158S-N	35.8	493.7	24.50	0.003654	0.001163	47	Shear
210S-N	45.9	389.4	18.08	0.002570	0.002355	41	Shear
NS-SF	56.2	411.1	17.90	0.002362	–	38	Shear

V_{cr} = initial shear crack, $V_{u, exp}$ = ultimate shear strength of experimental test, δ_u = deflection at peak load, ε_L = average maximum strain of longitudinal reinforcement measured by strain gages at bottom layer of the mod-span, ε_T = maximum strain of shear reinforcement by the strain gage at the outside of the center layer, θ_{exp} = measured angle of the inclination of the critical shear crack at beam mid-height.
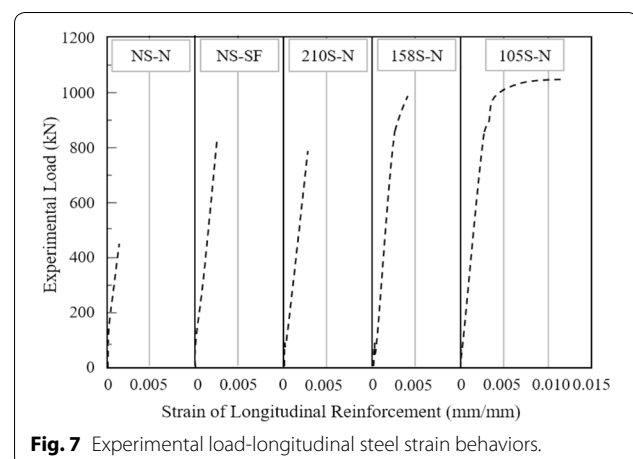
There are some limitation of using steel fiber reinforced concrete (SFRC) in beam member for shear resistance as recommended by ACI 318-19 (ACI Committee 318 2019). For the materials properties, the volume fraction of steel fiber should great than or equal to 0.75% and compressive strength not exceeding 40 MPa, and flexural strength (ASTM C1609M) at L/300 and L/150 should greater than or equal to 90% and 75% of the measured first-peak strength (f_{LOP}), respectively. For the beam member, height of beam section (h) and ultimate shear strength (V_u) should small than 600 mm and $\phi 0.17\sqrt{f_c'}b_w d$, respectively. In this study, the volume fraction of steel fiber, h, the flexural strength at L/300 and L/150 dose conform to the ACI 318-19, which were 0.75 vol%, 500 mm, 9.94 MPa (108%f_{LOP}), 8.34 MPa (91%f_{LOP}), respectively (Fig. 5a). Conversely, the compressive strength and experimental V_u exceeding the ACI 318-19 recommendation, which exhibited 72 MPa, 411 kN ($\phi 0.17\sqrt{f_c'}b_w d = 162.6$ kN), respectively. The interesting results of this study is that the 0.75 vol% steel fibers can be used as an alternative to instead of the minimum shear reinforcement in HSC beam, even though there are some different properties compared with ACI 318-19 recommendation.

The Fig. 6b shows the load relative to deflection behavior of different shear reinforcement spacing. In the specimens with shear reinforcement, the ultimate shear strength increased by at least 163.4 kN, 267.7 kN, and 311.8 kN, respectively. Due to reinforced by the close spacing of the shear reinforcement, the specimen 105S-N exhibited lower load of the initial shear crack, higher ultimate shear load and deflection at the peak load as 30.4 kN, 537.8 kN and 29.44 mm, respectively. The lower load of initial shear crack was observed with decrease in the shear reinforcement spacing, and high deflections occurred at the peak load and more ductile behavior after the peak load was obtained, which was similar to that in a recent study (Grünewald 2004). The maximum shear load of specimens indicates that the specimens with a close interval of shear reinforcement failed at a higher shear load. For example, the specimen 210S-N resisted the dominant shear crack based on only one shear reinforcement, although the specimen 158N-S engaged two shear reinforcements to resist the dominant shear crack. Additionally, it is interesting to note that the flexural stiffness of reinforced HSC beam was insignificantly influenced by the spacing of shear stirrups.

3.2.2 Load-Longitudinal Reinforcement Strain Relationship

The behavior of the load-strain variation in the longitudinal reinforcement was evaluated based on the strains measured by steel strain gages on the rebar surface as shown in Fig. 7. All of the specimens with shear reinforcement or steel fibers exhibited shear failure before the yielding of longitudinal reinforcing rebars with the exception of the specimen with a denser space of shear reinforcement, 105S-N, and 158S-N that exhibited the yielding of longitudinal reinforcing rebars (nethermost rebars). Additionally, the strain value of longitudinal reinforcement increased with decreases in shear reinforcement spacing, and high strain values occurred at specimen 105S-N with 0.008573 mm/mm (Table 8). Specimen NS-N exhibited a lower strain value due to the
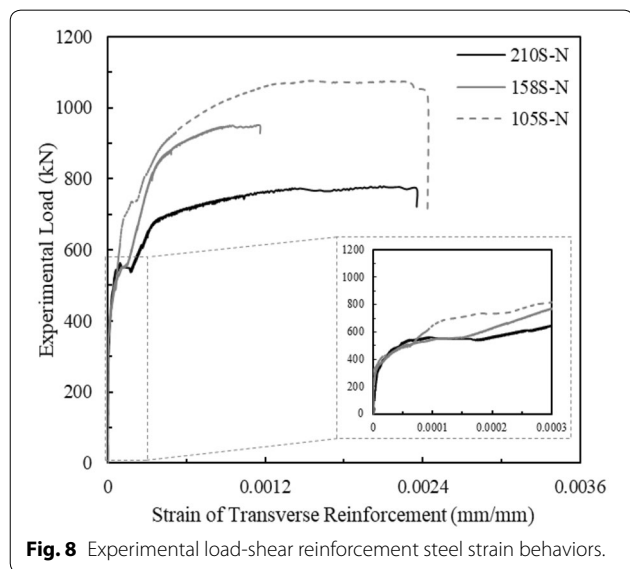

Fig. 7 Experimental load-longitudinal steel strain behaviors.

sudden shear failure of the concrete as expected with the absence of shear reinforcement and steel fibers. Furthermore, based on the excellent bond strength at the steel fiber with concrete matrix interface and fiber-bridging capability to control the crack development, the specimen NS-SF exhibited a lower strain value of longitudinal reinforcement as 0.002362 mm/mm, and it is approximately 8.1% lower when compared with 210S-N.

3.2.3 Load-Shear Reinforcement Strain Relationship
The reinforced HSC beams with shear reinforcing rebars for different spacings that are labeled as 105S-N, 158S-N, and 210S-N were considered to analyze the relationship between shear and stirrup strains. The progress of strain in the shear reinforcement of the specimens is shown in Fig. 8. Given the load-strain behavior, the strain increases very sharply with a slightly increase in the load after 0.0001 mm/mm strain of shear reinforcement. It was mainly caused by the formation of shear cracks, which occurred at approximately 560 kN during the experimental observation. Subsequently, a sudden increase in the shear load was observed for the 105S-N and 158S-N immediately after the formation of dominant shear cracks. However, this phenomenon was prevented by decreasing the spacing of shear stirrups due to the increased quantity of shear reinforcement to resist the dominant shear cracks. The yield strain values for the steel rebar under pullout test and shear test were very similar and approximately corresponding to 0.002330 mm/mm. Based on the steel gages attached to the side of the U-shear reinforcement surface to evaluate shear load relative to strain behavior, the shear load relative to strain behavior is represented accurately.

Fig. 8 Experimental load-shear reinforcement steel strain behaviors.

Additionally, extremely high deviation values occurred at times when the shear failure of shear reinforcement occurred on the side without the steel gage. Hence, the specimen 158S-N exhibited 50% lower strain values when compared with others after the shear failure of the test beam.
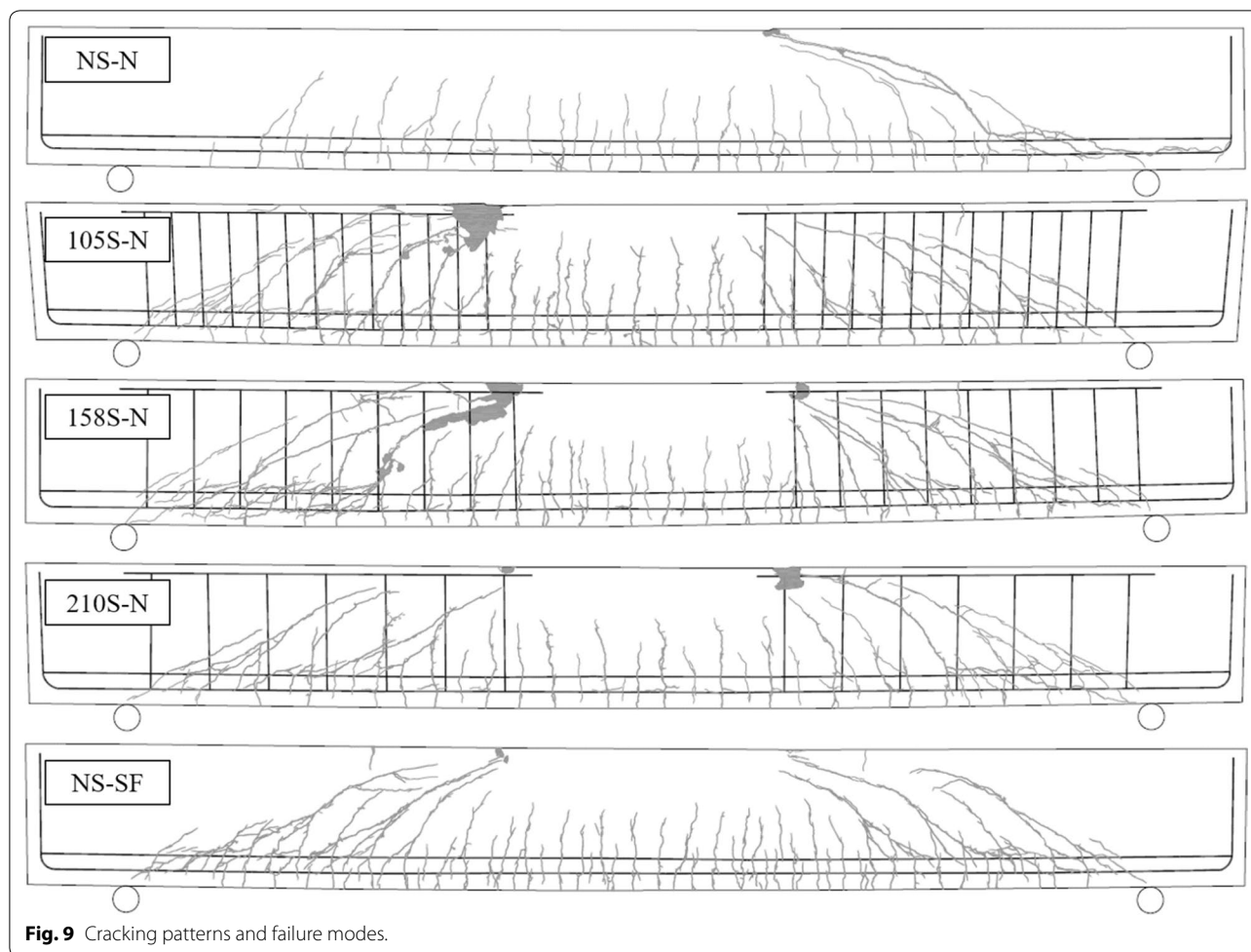
3.2.4 Crack and Failure Patterns
Figure 9 shows the propagation of cracks in all test beams. The test of crack and failure patterns of the beams were evaluated, and the propagation and width of cracks were evaluated at each loading step.

The initial cracking of test beams was observed under 60 kN and the load increased linearly from the beginning of the test to the initial shear crack (Fig. 6). The initial crack was observed at the bottom area of the beam between the two equal concentrated loading points where the beam was subjected to maximum stress. The initial crack occurrence was observed since an audible signal, and it exhibited barely visible cracks. New cracks occurred and developed after the initial crack under a continued loading. Additionally, most of the cracks continued to develop and increase (crack length) towards the upper area of the beam, and individual cracks slowly increased width. Subsequently, the typical shear cracks were displayed on the beam surface and a typical shear crack develops to the dominant shear crack until shear failure occurred.

The specimen without any reinforcement (NS-N) exhibited typical shear cracking behavior after 200 kN of the experimental load, and the typical shear crack occurred at a maximum shear load acting on the test beam. After the maximum shear load, shear failure suddenly occurred in specimen NS-N, which exhibited the very brittle behavior of shear failure. In order to avoid brittle fracture, shear reinforcement and three different reinforcement spacing were applied. The specimens (105S-N, 158S-N, and 210S-N) exhibited typical shear cracking behavior when the shear reinforcement approached a maximum value and the typical shear crack width evidently increased with increases in the load after yielding until shear failure.

The specimen NS-SF exhibited typical shear cracking behavior when the steel fiber began to pullout of the HSC matrix. When the load carried by individual steel fiber overcame the ability of the HSC to grip, the fiber was pulled out (Amin and Foster 2016; Sydney and Hanai 1997; Yang et al. 2010). The fibers were individually pulled out due to increases in the load. Based on the fiber bridging and energy dissipation effect, more cracks were formed and more stress was resisted at the existing cracks. Additionally, the typical shear crack occurred at a high load value interval (>600 kN) on test beams, and the

Fig. 9 Cracking patterns and failure modes.

typical shear crack width evidently increased when compared with other cracks. Finally, shear failure of the test beam occurred due to crack localization as a result of the pulling out of fibers.

Figure 10 shows the load relative to crack width and load relative to crack number curves. Each load step compared and recorded the crack width and number of cracks in the test with respect to the cracks visible to the naked eye.
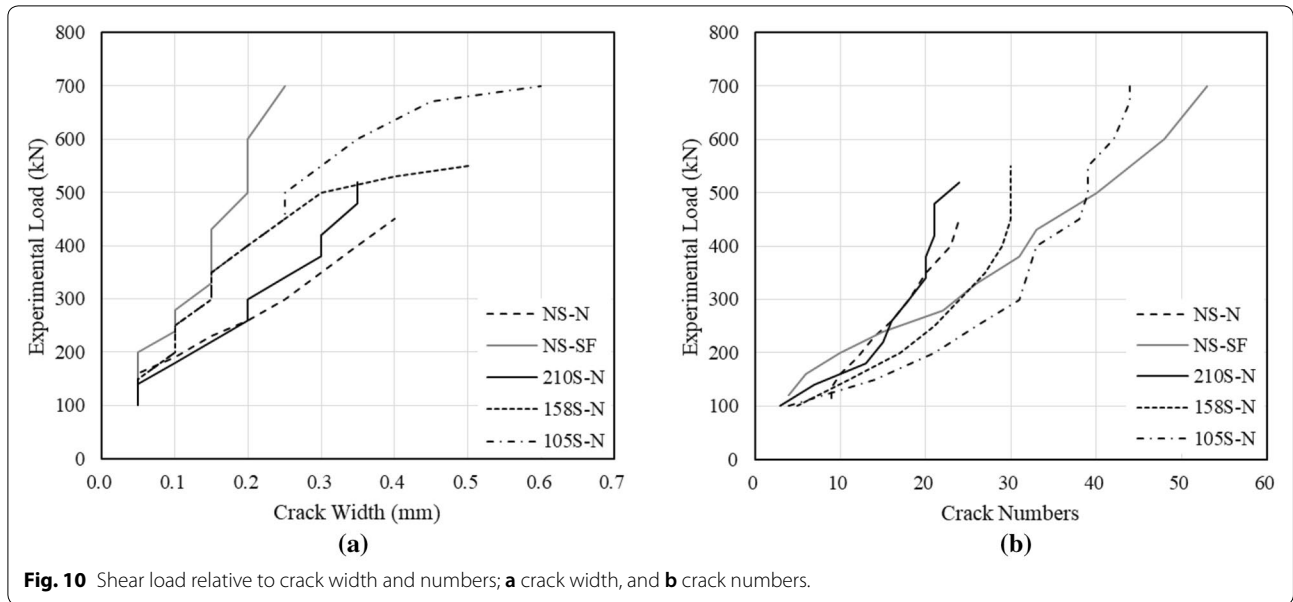
The HSC beam with steel fiber was more effective in controlling cracking under normal stress due to the occurrence of several close crack spacings when compared with the beam without steel fiber (NS-N) and with minimum shear reinforcement (210S-N). However, these were similar to those of specimen 158S-N. Based on the bonding stress at the fiber-matrix interface and the fiber bridging stress crossing the cracks, the specimen NS-SF exhibited several micro cracks with increases in the load when compared with NS-N and 210S-N after exhibiting a diagonal shear crack. Hence, the steel fibers acted effectively as minimum shear reinforcement and enhanced

strength and ductility of the HSC beam. Generally, the addition of fibers led to reductions in crack width and resulted in a more diffused cracking pattern (Aoude et al. 2012). Furthermore, in the HSC beams with shear reinforcement, the decrease in shear reinforcement spacing increased the intensity of the diagonal cracking, and the number of cracks increased with increases in the shear strength.

3.3 Comparison of Testing Shear Value and Prediction of Shear Strength

3.3.1 *Prediction of Shear Strength*
Several studies attempted to predict equations for the shear capacity of fiber RC beam to contribute to shear design method. Data analysis of several studies indicates that the behavior of SFRC beam remains a complex problem (Aoude et al. 2012; Foster 2010; Sharma 1986; Al-Ta'an and Al-Feel 1990; Swamy et al. 1993; Kuntia et al. 1999; Yakoub 2011; RILEM TC 162-TDF 2000b; AFGC 2013). All the proposed calculation methods for shear load capacity of beams were divided into

Fig. 10 Shear load relative to crack width and numbers; **a** crack width, and **b** crack numbers.

the following three terms: (1) shear resistance of the member without shear reinforcement due to the compression zone, longitudinal reinforcement, aggregate interlock et al., (2) contribution of shear reinforcement, (3) contribution of steel fibers, as shown in Eq. (1) as follows:

$$V_d = V_c + V_s + V_{fib} \qquad (1)$$

where V_d denotes the shear load capacity, V_c denotes the shear resistance of the member without shear reinforcement, V_s denotes the shear resistance of contribution of the shear reinforcement, and V_{fib} denotes the shear resistance of contribution of steel fibers.

Generally, in order to compute the shear strength of the reinforced concrete, the shear resistance of the concrete matrix is computed by using the following equation: $V_c = \emptyset_c \beta \sqrt{f_c'} b_w d_v$, where $b_w d_v$ denotes the effective shear area represented by the web width multiplied by the effective shear depth of beam. Additionally, the shear resistance of contribution of the shear reinforcement is based on the number of shear reinforcement.

Therefore, in this section, the ultimate shear strength obtained by the experimental investigation and the predicted value from design guidelines and that proposed by extant studies is compared (Table 9). These predictions of shear capacity for effect of fiber were mainly divided into the following two types: (1) separate from concrete contribution and accounted for by using fiber factor (Type 1), (2) included in concrete contribution and accounted for by using SFRC material properties in tension (Type 2). The predictions of shear strength by RILEM TC-TDF

Table 9 Summary of a typical predictions of shear strength.

Investigator/design guidelines	Shear strength model, kN
Sharma (1986)	$V_{fib, SAK} = kf_t(d/a)^{0.25}$
Al-Ta'an and Al-Feel (1990)	$V_{fib, AT} = \frac{8.5}{9} k_f (V_f \frac{L_f}{d_f}) b_w d$
Swamy et al. (1993)	$V_{fib, SRN} = 0.37\tau(V_f \frac{L_f}{d_f}) b_w d$
Khuntia et al. (1999)	$V_{fib, KM} = 0.25\beta(V_f \frac{L_f}{d_f})\sqrt{f_c} b_w d$
Foster (2010)	$V_{fib, FSJ} = 0.9 k_{fd} f_w b_w d cot\theta$
Aoude et al. (2012)	$V_{fib, HA} = 0.83 F_p N_{fib} b_w d_v cot\theta$
Yakoub (2011)	$V_{fib, YHE} = 2.5\beta\sqrt{f_c}(1 + 0.70 V_f \frac{L_f}{d_f} R_g)\frac{d}{a}$ for $\frac{a}{d} \leq 2.5$
	$V_{fib, YHE} = \beta\sqrt{f_c}(1 + 0.70 V_f \frac{L_f}{d_f} R_g)$ for $\frac{a}{d} > 2.5$
RILEM TC 162-TDF (2000)	$V_{fib, RIL} = k_f k_l \tau_{fib} b_w d$
AFGC 2013 (2013)	$V_{fib, AC} = (0.9 b_w d\sigma_{Rdf})tan\theta$
Spinella (2013)	$V_{fib, SN} = 0.22 v_o f_{cf} h/[(a-x_0) b_w d_w]$

recommendation (RILEM TC 162-TDF 2000b) and Hassan et al. (Aoude et al. 2012) is a typical equation for each concept.

The RILEM TC 162-TDF recommendation (Yakoub 2011) that is a very widely used code for SFRC, and it was proposed to predict the equation for shear resistance of contribution of the shear reinforcement ($V_{fib,RIL}$). It is based on the use of more than 100 test data of SFRC beam to establish a predictive relation for $V_{fib,RIL}$, and to verify against the possibility of occurrence of a failure state similar to that of plain concrete (Lucie 2000; Vandewalle 2000). The details of the equation are as follows:

Yuan *et al. Int J Concr Struct Mater* (2020) 14:21

Page 12 of 15

$$V_{fib,R} = k_f k_l \tau_{fib} b_w d \tag{2}$$

$$k_f = 1 + n \left(\frac{h_f}{b_w} \right) \left(\frac{h_f}{d} \right) \le 1.5 \tag{3}$$

$$n = \frac{b_f - b_w}{h_f} \text{ where } n \le 3 \text{ and } \frac{3b_w}{h_f} \tag{4}$$

where k_f denotes the factor taking into account the contribution of the beam section, h_f denotes effective depth of the section, b_f denotes width of the flanges, b_w denotes width of the web, k_l is equal (1600-d)/1000 and greater than or equal to 1, and τ_{fib} denotes the design value of the increase in shear strength due to steel fibers ($0.12f_{eqk,3}$).

Aoude et al. (2012) suggested a prediction equation of shear strength resistance with respect to the contribution of steel fibers ($V_{fib,HA}$) that is related to the pullout strength of the fibers crossing cracking plane and fibers randomly oriented in three dimensions. Additionally, a crack inclination θ of the SFRC beam was considered under the free body diagram. Thus, the $V_{fib,HA}$ was calculated as follows.

$$V_{fib,HA} = 0.83 F_P N_{fib} b_w d \cot\theta \tag{5}$$

$$F_P = \left(\tau_{fib} \pi d_f \frac{L_f}{2} \right) + \Delta P' \tag{6}$$

$$N_{fib} = \frac{v_f}{A_f} \alpha \eta_l \tag{7}$$

where F_P denotes the pullout strength of hooked-end steel fiber, τ_{fib} denotes the bond strength between fiber and concrete matrix, d_f denotes the fiber diameter, L_f denotes fiber length, $\Delta P'$ denotes the effect of hooked-end steel fiber on pullout test, N_{fib} denotes the fibers randomly oriented in three dimension, v_f denotes the volume fraction of fibers in the matrix, A_f denotes the cross-sectional area of the fiber, a and η_l denotes the orientation factor and length factor of the fiber, respectively.

With respect to the hooked-end steel fibers used in this study, the effect of the hook ($\Delta P'$) is examined on the pullout test by debonding of the fiber that is the mechanical effect of the hook in the straightening process of the fiber on the pullout from the matrix (Aoude et al. 2012; Alwan et al. 1999). This parameter is calculated as follows:

$$\Delta P' = \frac{3.05}{\cos(45° \times \pi/180°)} \left(f_y \frac{\pi(d_f/2)^2}{6} \right) \tag{8}$$

where f_y denotes the fiber yield strength.

In this study, the average bond strength (τ_{fib}) was obtained as 6.16 MPa, which is based on single fiber pull-out test results (Fig. 5b). The fiber orientation factor (a) and length factor (η_l) were suggested by using 3/8 and 0.5, respectively (Foster 2001; Aoude 2007).

3.3.2 Comparison of Shear Strength

Table 10 compares the shear strength value between experimental and prediction equations. The HSC beams without steel fiber and shear reinforcement exhibited 226.0 kN shear strength (Table 8), which is approximately the pure shear strength of the concrete beam. In the HSC beams with shear reinforcement, the shear resistance capacity of shear reinforcement ($V_{s, TR}$) was calculated by Eq. (1), and the values of specimens with increases in shear reinforcement ratios were 163.4 kN, 267.7 kN, and 311.8 kN, respectively. Therefore, the shear resistance capacity increases with increases in the shear reinforcement ratios, which were approximately 63.8% and 90.8% higher than those of $V_{s, 0.16}$ (minimum shear reinforcement). Additionally, the shear resistance capacity of steel fibers in the specimen with steel fibers is 185.1 kN, which approximately increases shear resistance by 13.2% when compared with the HSC beam with minimum shear reinforcement ($V_{s, 0.16}$). Therefore, given the test results, the HSC use of fiber volume fraction of 0.75% can replace the minimum shear reinforcement through the use of hooked steel fibers as recommended by the ACI 318-19 Code.

A comparison of the predicted shear strength using the proposed Type 1 equation and the experimental value, due to consider only a factor influencing the factor reflecting the fiber shape (k) or specific pullout tests on the FRC (τ), the predicted shear strength through equation $V_{fib, AT}$ and $V_{fib, SRN}$ resulted approximately 38.7–52.5% lower than $V_{fib, exp}$. The predicted shear strength through equation $V_{fib, KM}$ and $V_{fib, YHE}$ were close to the experimental values although they also below 16.5% of the suitable value when compared with $V_{fib, exp}$. It is based on considering an additional factor, namely the factor of fiber shape and concrete type (strength). Additionally, the equation $V_{fib, HA}$ considered more than five factors in the FRC, namely fiber orientation factor, fiber length factor, bond-shear strength between fiber and matrix, the contribution of the hook to fiber pull out strength, and angle of inclination of the shear crack. Hence, the predicted value of $V_{fib, HA}$ only varied by 10.9% and was very closer to $V_{fib, exp}$.

Furthermore, when compared to the predicted shear strength that used the proposed Type 2 equation and experimental value, the following are obtained: the predicted shear strength equations were mainly accounted for by using steel fiber reinforcement concrete material properties in tension, which was based on the direct

Table 10 Summary of predictions of the shear resistance of contribution of steel fibers.

	$V_{s,\,TR}$ (kN)	V_{fib} (kN)	$V_{s,\,fib}/V_{fib,\,exp}$ (%)	Remarks
Type 0				
$V_{fib,\,exp}$	–	185.1	100	Fiber effect is:
$V_{s,\,0.16}$	163.4	–	88.3	• calculated by experimental value
$V_{s,\,0.21}$	267.7	–	144.6	
$V_{s,\,0.32}$	311.8	–	168.4	
Type 1				
$V_{fib,\,AT}$	–	71.7	38.7	Fiber effect is:
$V_{fib,\,SRN}$	–	97.2	52.5	• separate from concrete contribution
$V_{fib,\,KM}$	–	135.0	72.9	• accounted for by using fiber factor
$V_{fib,\,HA}$	–	205.3	110.9	
$V_{fib,\,YHE}$	–	154.5	83.5	
Type 2				
$V_{fib,\,SAK}$	–	93.2	50.4	Fiber effect is:
$V_{fib,\,FSJ}$	–	83.9	45.3	• included in concrete contribution
$V_{fib,\,RIL}$	–	53.1	28.7	• accounted for by using SFRC material properties in tension
$V_{fib,\,AC}$	–	81.4	44.0	
$V_{fib,SN}$	–	58.9	31.8	

$V_{s,TR}$ = the shear resistance of stirrups based on difference transverse reinforcement ratio, V_{fib} = the shear resistance of contribution of steel fibers, $V_{s,\,fib}$ = the shear resistance of contribution of transverse reinforcement or calculated by prediction equation, $V_{fib,\,exp}$ = the shear resistance of contribution of steel fibers by experimental test, $V_{s,\,0.16}$, $V_{s,\,0.21}$, $V_{s,\,0.32}$ = the transverse reinforcement ratios under different stirrup spacing which 0.5d, 0.375d, and 0.25d, respectively.

tensile or bending test. Therefore, the predicted shear strength values were less more than 50% when compared with the actual experimental value ($V_{fib,\,exp}$). Proving, once again, the predict shear strength using Type 2(accounted for by using material properties by tensile test) may lead to high data error.

Given the fore-mentioned equations, the $V_{fib.HA}$ exhibited a more closes predicted shear strength value with a 10.9% difference in experimental values. A modification factor of 0.83 was employed in the equation as used by extant studies in normal strength concrete, and a size effect may play a role in reducing the shear resistance of test beams. Thus, modification factor and size effect should be determined for the optimal prediction of an equation to design the shear strength of the HSC with steel fibers in a future study.

4 Conclusions

An experimental investigation was performed to evaluate the shear behavior of HSC beams with different reinforcements. Five large-scale reinforced HSC beams were tested under four-point loading. One of test beam was reinforced with 0.75 vol% of hooked steel fibers without shear reinforcements to evaluate the feasibility of replacing minimum shear reinforcement as recommended by the ACI 318-19 Code. Four other test specimens were reinforced with different shear reinforcement ratios of 0.0, 0.16, 0.21 and 0.32, respectively. Based on the results

of this investigation, the following concluding remarks are obtained:

1. When compared to the plain HSC, the steel fiber reinforced HSC exhibited higher compressive strength, flexural strength, and energy absorption capacity based on the restraint of micro-crack propagation.
2. All the five large-scale specimens finally exhibited failure by the shear failure mode. The shear strength, deflection at capacity, and angle of shear crack increased with a decrease in the shear reinforcement spacing.
3. When compared to the reinforced HSC beams with stirrups or steel fibers, the steel fiber reinforced HSC beam without stirrups exhibited higher shear strength albeit lower ultimate deflection capacity of approximately 5.6% and 1.1%, respectively. Thus, the use of minimum hooked steel fibers in HSC beam is effective in controlling shear cracks.
4. The shear resistance capacity of the beam with steel fibers exhibited 185.1 kN is approximately 13.2% higher when compared with that of the HSC reinforced with minimum shear reinforcement. Hence, the 0.75 vol% steel fibers can be used as an alternative to instead of the minimum shear reinforcement in HSC beam, even though there are some different properties compared with ACI 318-19 recommendation.

Yuan *et al. Int J Concr Struct Mater*   (2020) 14:21

Page 14 of 15

5. When compared to the shear strength of concrete beam between the experimental and prediction equations (Type 1 and Type 2), V_{fib} calculated by Type 1 prediction equations were more close to experimental value than those of Type 2. Especially, Hassan's model was most similar to $V_{fib, exp}$ (110.9% $V_{fib, exp} = V_{fib.HA}$), but it was inadequate in predicting the shear strength of reinforced HSC beam with steel fibers. Thus, modification factor and size effect should be improved for the optimal prediction of shear capacity of HSC with steel fibers in a future study.

Abbreviations

b_w: width of the test beam; d_v: effective shear depth; d_f: fiber diameter; d/a: the effective depth-to-shear span ratio; f_c, f_{cf}: concrete strength; f_t: the tensile strength of concrete; f_w: tensile strength exhibited by the steel fibers over a plane of the unit area; F_p: fiber pullout strength; k: conversion coefficient of the tension strength of concrete; k_f: factor reflecting the fiber shape; k_{fd}: fiber dispersion reduction factor; k_l: (1600-d)/1000; L_f: fiber length; N_{fib}: fibers randomly oriented in three dimensions; V_f: fiber-volume ratio; R_g: fiber geometry factor; x_0: distance between the support and critical crack; $\sigma_{Rd,f}$: the residual tensile strength of the fiber-reinforced cross section; τ: the bond-shear strength of the concrete matrix strength; τ_{fib}: 0.12 times of flexural tensile strength $f_{eq,3}$, $(0.12f_{eq,3})$; θ: the angle of inclination of the shear crack; β: factor for fiber shape and concrete type; v_0: effectiveness factors for concrete in compression.

Authors' contributions

T-FY and Y-SY conceived and designed the experiments; T-FY, D-YY and J-MY performed the experiments; T-FY analyzed the experimental data and wrote the manuscript. All authors read and approved the final manuscript.

Availability of data and materials

The data used to support the findings of this study are available from the corresponding author upon request.

Competing interests

The authors declare that they have no competing interests.

Author details

[1] School of Civil, Environmental and Architectural Engineering, Korea University, 145 Anam-ro, Seongbuk-gu, Seoul 02841, Republic of Korea. [2] Department of Architectural Engineering, Hanyang University, 222 Wangsimni-ro, Seongdong-gu, Seoul 04763, Republic of Korea. [3] Department of Civil Engineering, Keimyung University, 1095 Dalgubeol-daero, Dalseo-gu, Daegu 42601, Republic of Korea.

References

Abu-Lebdeh, T., Hamoush, S., Heard, W., & Zornig, B. (2011). Effect of matrix strength on pullout behavior of steel fiber reinforced very-high strength concrete composites. *Construction and Building Materials, 25*(1), 39–46.

ACI Committee 318. (2019). *Building code requirements for structural concrete (ACI 318-19) and commentary (318R-19)*. Farmington Hills: American Concrete Institute.

AFGC 2013. (2013). *Ultra high-performance fiber reinforced recommendations*. The AFGC's Scientific and Technical Committee.

Al-Ta'an, S. A., & Al-Feel, J. R. (1990). Evaluation of shear strength of fiber-reinforced concrete beams. *Cement and Concrete Composites, 12*(2), 87–94.

Alwan, J. M., Naam, A. E., & Guerrero, P. (1999). Effect of mechanical clamping on the pull-out response of hooked steel fibers embedded in cementitious matrices. *Concrete Science and Engineering, 1*, 15–25.

Amin, A., & Foster, S. J. (2016). Shear strength of steel fiber reinforced concrete beams with stirrups. *Engineering Structures, 111*, 323–332.

Aoude, H. (2007). *Structural behavior of steel fiber reinforced concrete members* (Ph.D. thesis) p. 269.

Aoude, H., Belghiti, M., Cook, W. D., & Mitchell, D. (2012). Response of steel fiber-reinforced concrete beams with and without stirrups. *ACI Structural Journal, 109*(3), 359–367.

ASTM C 39/C39M. (2014). *Standard test method for compressive strength of cylindrical concrete specimens* (pp. 1–7). West Conshohocken, PA: ASTM International.

ASTM C1609/C1609M. (2012). *Standard test method for flexural performance of fiber-reinforced concrete (using a beam with third-point loading)* (pp. 1–9). West Conshohocken, PA: ASTM International.

Bentz, E. C., Vecchio, F. J., & Collins, M. P. (2006). The simplified MCFT for calculating the shear strength of reinforced concrete elements. *ACI Structural Journal, 103*(4), 614–624.

Cucchiara, C., La Mendola, L., & Papia, M. (2004). Effectiveness of stirrups and steel fibers as shear reinforcement. *Cement and Concrete Composites, 26*(7), 777–786.

Ezeldin, A. S., & Balaguru, P. N. (1992). Normal-and high-strength fiber-reinforced concrete under compression. *Journal of Materials in Civil Engineering, 4*(4), 415–429.

Fettu, R. (2008). Fiber reinforced concrete: Design and application. In BEFIB 2008. Bangneux, France: RILEM Publication S.A.R.L. PRO60.

Foster, S. J. (2001). On the behavior of high-strength concrete columns: Cover spalling, steel fibers, and ductility. *ACI Structural Journal, 98*(4), 583–589.

Foster, S. J. (2010). Design of FRC beams for shear using the VEM and the draft model code approach. *Fib Bulletins, 57*, 195–210.

Grünewald, S. (2004). *Performance-based design of self-compacting fiber reinforced concrete* (Ph.D. thesis, Department of Structural and Building Engineering, Delft University of Technology, Delft, the Nether-lands) p. 165.

Khuntia, M., Stojadinovic, B., & Goel, S. C. (1999). Shear strength of normal an high strength fiber reinforced concrete beams without stirrups. *ACI Structal Journal, 96*(2), 282–289.

Lantsoght, E. O. L. (2019). How do steel fibers improve the shear capacity of reinforced concrete beams without stirrups? *Composites Part B: Engineering, 175*, 107079.

Lucie, V. (2000). Design method for steel fiber reinforced concrete proposed by RILEM TC 162-TDF. In Fifth Inter RILEM Symp FRC (pp. 51–64).

Minelli, F., & Plizzari, G. A. (2013). On the effectiveness of steel fibers as shear reinforcement. *ACI Structural Journal, 110*(3), 379–389.

Naaman, A. E., & Reinhardt, H. W. (2006). Proposed classification of HPFRC composites based on their tensile response. *Materials and Structures, 39*(5), 547–555.

Narayan, R., & Darwish, I. (1987). Use of steel fibers as shear reinforcement. *ACI Structural Journal, 84*(3), 216–227.

Noghabai, K. (2000). Beams of fibrous concrete in shear and bending: Experiment and model. *Journal of Structural Engineering, 126*(2), 243–251.

Oesterreich, T. D., & Teuteberg, F. (2016). Understanding the implications of digitization and automation in the context of industry 40: A triangulation approach and elements of a research agenda for the construction industry. *Computers in Industry, 83*(December), 121–139.

Parra-Montesinos, G. J., & Wight, J. K. (2006). Shear strength of beams with deformed steel fibers. *Concrete International, 28*(11), 57–66.

Prisco, M., Plizzari, G., & Vandewalle, L. (2009). Fiber-reinforced concrete-new design perspectives. *Materials and Structures, 42*(9), 1261–1281.

RILEM TC 162-TDF. (2000a). Test and design methods for steel-fibre-reinforced concrete: Bending test. *Materials and Structures, 33*(225), 3–5.

RILEM TC 162-TDF. (2000b). Test and design methods for steel-fibre-reinforced concrete. *Materials and Structures, 33,* 75–81.

Sahoo, D. R., Maran, K., & Kumar, A. (2015). Effect of steel and synthetic fibers on the shear strength of RC beams without shear stirrups. *Construction and Building Materials, 83,* 150–158.

Sharma, A. K. (1986). Shear strength of steel fiber reinforced concrete beams. *ACI Journal, 83*(4), 530–538.

Spinella, N. (2013). Shear strength of full-scale steel fiber-reinforced concrete beams without stirrups. *Computers and Concrete, 11,* 365–383.

Swamy, R. N., Jones, R., & Chiam, A. T. P. (1993). Influence of steel fibers on the shear resistance of lightweight concrete T-beams. *ACI Structural Journal, 90*(1), 103–114.

Sydney, F. J., & Hanai, J. B. D. (1997). Shear behavior of steel fiber reinforced concrete beams. *Cement and Concrete Composites, 19,* 359–366.

Tan, K. H., Murugappan, K., & Paramasivam, P. (1993). Shear behavior of steel fiber reinforced concrete beams. *ACI Structural Journal, 90*(1), 3–11.

Vandewalle, L. (2000). Recommendation of RILEM TC 162-TDF: Test and design methods for steel fibre reinforced concrete: σ-ε design method. *Materials and Structures, 33*(226), 75–81.

Won, J. P., Hong, B. T., Lee, S. J., & Choi, S. J. (2013). Bonding properties of amorphous micro-steel fiber-reinforced cementitious composites. *Composite Structures, 102,* 101–109.

Yakoub, H. E. (2011). Shear stress prediction: Steel fiber-reinforced concrete beams without stirrups. *ACI Structal Journal, 108*(3), 304–314.

Yang, I. H., Joh, C., & Kim, B. S. (2010). Structural behavior of ultra-high performance concrete beams subjected to bending. *Engineering Structures, 32,* 3478–3487.

Yang, J. M., Yoo, D. Y., Kim, Y. C., & Yoon, Y. S. (2017). Mechanical properties of steam cured high-strength steel fiber-reinforced concrete with high-volume blast furnace slag. *International Journal of Concrete Structures and Materials, 11*(2), 391–401.

Yoo, D. Y., Yuan, T. F., Yang, J. M., & Yoon, Y. S. (2017). Feasibility of replacing minimum shear reinforcement with steel fibers for sustainable high-strength concrete beams. *Engineering Structures, 147,* 207–222.

Yuan, T. F., Yang, J. M., Kim, K. D., & Yoon, Y. S. (2018). Evaluating strength development and durability of high-strength concrete with 60% of ground-granulated blast furnace slag. *Journal of the Korean Society of Hazard Mitigation, 18*(7), 307–314.

Zezulka, F., Marcon, P., Vesely, I., Sajdl, O. (2016). *Industry 4.0-An introduction in phenomenon*. In 14th IFAC conference on programmable devices and embedded systems PDES *49*(25) 8–12.

Publisher's Note